A HIGH-RESOLUTION HINDCAST OF THE FLOODING DURING XYNTHIA STORM, CENTRAL BAY OF BISCAY

Kai Li[1], Xavier Bertin[2], Aron Roland[3], Yinglong J. Zhang[4] and Jean-François Breilh[5]

Abstract

The Xynthia Storm severely hit the central of Bay of Biscay in February 2010. Large areas of low-lying coast were flooded, causing large economic and live losses. The innovative fully coupled wave-current modelling system SELFE/WWMII was developed and applied to hindcast the flooding associated with Xynthia. The comparison with available wave and water level data revealed that these parameters as well as the extension of the flooding were well reproduced by our modelling approach. The analysis of the modelling results improves understanding of the physical processes which control the storm surge and the coastal flooding. This better understanding will contribute to improve the prediction and prevention of potential damage associated with future storms.

Keywords

flooding grid, storm surge, Xynthia, SELFE, WWMII

1. Introduction

Storm surges correspond to abnormal variations in the ocean free-surface driven by atmospheric and oceanic forcing associated with extra-tropical storms or tropical hurricanes and typhoons (Flather, 2001). At low-lying coasts, the largest damages are generally associated with storm surges and the subsequent flooding rather than direct wind effects, particularly if the surge coincides with high spring tides. According to shallow water equations, the wind effect is inversely proportional to the water depth, which causes the wind effect to be dominant over atmospheric pressure gradients in shallow waters. Low-lying coasts bordered by extensive continental shelves and exposed to hurricanes and storms are thus particularly vulnerable to coastal flooding. The Bay of Bengal and the Gulf of Mexico combine these settings and are the regions in the world where the deadliest hurricane-induced flooding has been reported. To a lesser degree, North-Western Europe is also susceptible to storm surge and coastal flooding risks. Actually, this region is located on the path of mid-latitude depressions and combines low-lying barrier islands, wetlands and estuaries surrounded by large continental shelves. The most dramatic catastrophe in the modern history took place in the North Sea in 1953, where a severe storm surge locally exceeding 3.0 m and peaked at the same time as a high spring-tide (Gerritsen, 2005). The subsequent extreme water level caused the breaching of 150 sea-

[1] LIENSS, University of La Rochelle, 2 rue Olympe de Gouges, La Rochelle 17000, France. kli@univ-lr.fr
[2] LIENSS, University of La Rochelle, 2 rue Olympe de Gouges, La Rochelle 17000, France. xbertin@univ-lr.fr
[3] Institute for Hydraulic and Water Resources Engineering, Darmstadt University of Technology, Darmstadt. Germany. aaronroland@gmx.de
[4] Virginia Institute of Marine Science, Gloucester Point, Virginia, USA. yjzhang@vims.edu
[5] LIENSS, University of La Rochelle, 2 rue Olympe de Gouges, La Rochelle 17000, France. jbreil01@univ-lr.fr

dykes and the flooding of low-lying regions inhabited by about 750,000 people, 1836 of whom passed away tragically. In the Bay of Biscay, the Xynthia Storm severely hit the coastlines of Charente-Maritime and Vendée in the night between the 27th and the 28th February 2010. The associated storm surge exceeded 1.5 m at La Rochelle tide gauge while being in phase with a high spring tide, which caused the overall sea-level to reach the exceptional value of 8.0 m above marine chart datum (Bertin et al., 2012). Numerous dykes and dunes were flooded or breached and large coastal areas were flooded. More than 45 people died and material damages exceeded 2.0 billion Euros.

Storm surges are being investigated using numerical models since the mid nineteen sixties (Jelesnianski, 1965, 1966; Miyazaki, 1965; Miyazaki and Okada, 1975), which resulted in abundant literature on the mechanisms controlling this phenomenon. For instance, Hans et al., (1995) showed that, in storm surge models, the adequate representation of the dominant physical processes was more important than the numerical methods to solve the corresponding equations. For instance, accounting for the sea-state to compute the surface stress was shown to be essential to properly predict storm surges (Geernaert, et al., 1986; Mastenbroek, et al., 1992; Bertin et al., 2012). Once oceanic water levels are correctly reproduced, the simulation of associated flooding usually requires employing a high spatial resolution (Shen et al., 2006, 2006). For complex geometries, models using unstructured meshes were shown to be particularly adequate (Bilskie et al., 2012; Chen et al., 2008). Also, it was shown that the flooding distribution can be improved if land/ground nature is taken into account (Bunya et al., 2010) or taking into account subgrid unresolved features statistically (Milzow and Kinzelbach, 2010). However, research on flooding showed that, in some cases, the largest uncertainties originate rather from the forcing inputs of the flood model (e.g. coastal water levels and sea defense failures), rather than its internal boundaries, such as the model terrain and bottom friction (Brown et al. 2007). Recently, the better understanding of oceanic physical processes together with an exponential growth of computational capacities have permitted the development of sophisticated modelling systems capable of efficiently simulating storm surges and flooding with a high resolution over large geographical extensions (e.g. Bunya et al., 2010; Dietrich et al., 2010). Nevertheless, such an approach constitutes a multi-scale and very challenging problem because: (1) large geographical extend should be modeled to adequately reproduce wave development and atmospheric pressure effect; (2) very high resolution (i.e. <10 m) should be employed locally to represent correctly dykes and natural barriers; (3) efficient and very stable numerical methods should be employed to deal with the subsequent large variability of Courant numbers, large spatial gradients and wetting and drying. The purpose of this study is to present the application of a fully-coupled high-resolution innovative modelling system to hindcast the flooding associated with Xynthia.

2. **Study area**

2.1. Geomorphic setting

The modelling area covers the NE Atlantic Ocean, but this study is focused on the central part of Bay of Biscay, Western France. This area is called Pertuis Charentais and consists of estuaries and tidal bays sheltered from the open ocean by two main islands: Island of Ré and Island of Oléron (figure 1). The connection with the Atlantic Ocean is made through three segments of incised valleys: Pertuis Breton (12 km width), Pertuis d'Antioche (12 km width) and Maumusson Inlet (1 km width in the narrowest part). Several small rivers flow within Pertuis Charentais but freshwater discharges are usually negligible compared to tidal prisms. To the South, the Gironde Estuary corresponds to the largest estuary in Europe and the yearly-mean associated freshwater discharge is of the order of 900 $m3 \cdot s^{-1}$ (Castaing, 1981). In west of the Pertuis Charentais, the continental shelf of Bay of Biscay is around 180 km wide.

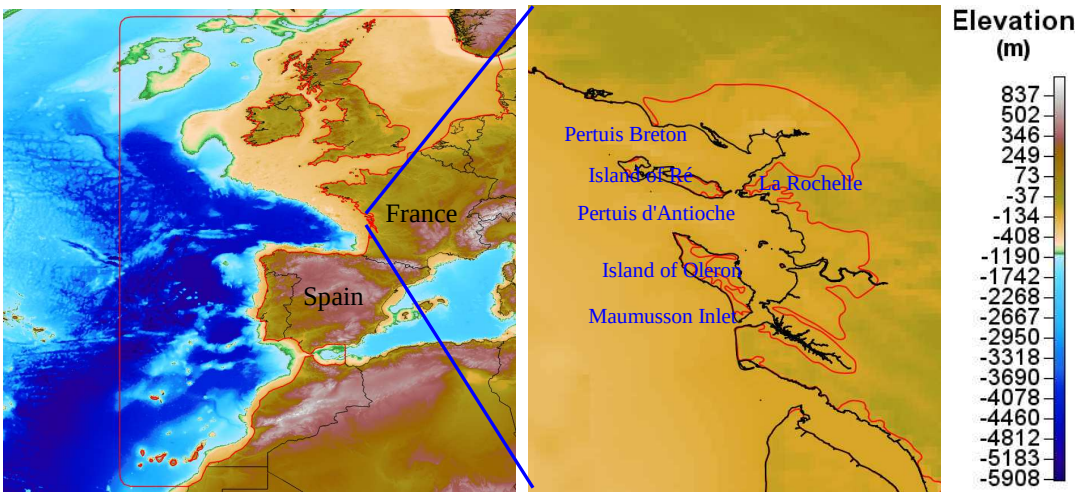

Figure 1. Location and bathymetry of the study area. The redline corresponds to the extent of the unstructured mesh.

2.2. Hydrodynamic setting

The circulation in the area around La Rochelle is dominated by semi-diurnal tides with small diurnal asymmetries. The spring tidal range can exceeds 6 m while the neap tidal range can fall below 2m. The amplitude of M2 increases from about 1 m over the abyssal plain to 1.80 m in Pertuis Breton (Le Cann, 1990; Bertin, 2012). The diurnal waves K1 and O1 have amplitude of 0.07 m and quarter diurnal waves M4, MS4 and MN4 experience a huge amplification after propagation through the central part of continental shelf due to a resonant process (Le Cann, 1990; Bertin et al., 2012). The western part of the islands is exposed to energetic gravity waves, predominantly coming from W to NW. The annual-mean significant wave height is of the order of 1.5 m in front of the Islands with peak periods typically ranging from 8 to 12 s, although winter storms episodically produce waves larger than 9 m (Bertin et al., 2008).

3. Data and Methods

3.1. Field data

Water level data were retrieved at three stations within the study area operating during Xynthia from SONEL (http://www.sonel.org) and REFMAR (http://refmar.shom.fr/fr/) databases. Wave conditions during Xynthia were characterized by means of a Datawell wave rider, deployed by SHOM (French Naval Oceanographic Service) to the west of Oléron Island (35 m water depth). The horizontal extension of flooded areas was determined combining images from SPOT 4 (10 meters resolution, taken two days after the storm), ENVISAT ASAR (12.5 meters resolution, taken two days after the storm), RADARSAT 2 (6 meters resolution, taken 4 days after the storm) satellites and field observations of storm deposits, physical marks or markers and damages on vegetation (DDTM-17, 2011).

3.2. Modelling system description

3.2.1. General outline

SELFE/WWMII (http://ccrm.vims.edu/w/index.php/Main_Page) is an open-source community modelling system fully-coupled and parallelized, using innovative numerical framework that can be used to investigate coastal circulation under the combined effects of tides, waves, atmospheric forcing and freshwater discharge at a large range of geographical scales (Roland et al., 2012). SELFE/WWMII is parallelized with MPI (Message Passing Interface) via domain decomposition using ParMETIS. SELFE and WWMII utilize the same unstructured triangular grid and same domain decomposition in the horizontal dimension. This coupling strategy combined with innovative numerical methods makes the modelling system hu efficient and allows massive parallel techniques.

3.2.2. Wave Model

WWMII is a 3rd generation spectral wave model that solves the Wave Action Equation, describing growth, decay, advection and refraction of wind waves due to depths and currents (computed by the hydrodynamic model). It includes various parameterization source terms, including Ardhuin TEST441, Ardhuin TEST442 (Ardhuin, 2010), ECMWF Cycle4 (Bidlot et al. 2007). Advection of wave action in geographical space is solved using the N-Scheme of Abgrall et al. (2006) while advection in spectral space is solved in a similar manner as in WWIII (Tolman, 2009). The wave action equations and source terms of WWMII are given as follows.

$$\frac{\partial}{\partial t} N + \nabla x(\dot{X} N) + \frac{\partial}{\partial \sigma}(\dot{\theta} N) + \frac{\partial}{\partial \theta}(\dot{\sigma} N) = S_{tot} \tag{1}$$

$$N_{(t,\mathbf{X},\sigma,\theta)} = \frac{E_{(t,\mathbf{X},\sigma,\theta)}}{\sigma} \tag{2}$$

Where N is the wave action, σ is the relative wave frequency, θ is the wave direction, X is the Cartesian coordinate vector (x, y) in the geographical space, $\dot{\theta}$ and $\dot{\sigma}$ are the rate of change of wave action in direction and frequency, respectively. S_{tot} is the sum of the source terms, which include input due to wind, nonlinear interaction in shallow water, nonlinear interaction in deep water, dissipation due to whitecapping, depth-limited breaking and bottom friction.

3.2.3. Circulation Model

SELFE uses an efficient semi-implicit time stepping algorithm in conjunction with an Eulerian-Lagrangian method (ELM) to treat the advection. It is robust and less dependent on CFL condition than other models (Zhang and Baptista, 2008). The continuity equation is solved using a hybrid finite-element/finite-volume method and the momentum equations are solved using a Galerkin finite element method based on an unstructured grid. For the vertical discretization, SELFE utilizes S-Z or pure S coordinates. Although the code can simulate baroclinic circulations and non-hydrostatic effects, SELFE was used in 2DH barotropic mode in this study. Thereby, the corresponding equations are the following:

$$\frac{\partial \eta}{\partial t} + \nabla \cdot (\mathbf{u} H) = 0 \tag{6}$$

$$\frac{D\mathbf{u}}{Dt} = \hat{f} - g\nabla\eta + f(v, -u) + \frac{\boldsymbol{\tau}_w - \boldsymbol{\chi}\mathbf{u}}{H} \tag{7}$$

$$\hat{f} = -\frac{1}{\rho_0}\nabla p_A + \hat{\alpha} g \nabla \psi + R_s + \hat{\tau}_S \tag{8}$$

$$\tau_w = (\rho_a u_*^2) \tag{9}$$

Where η is the free surface elevations, ∇ is the gradient operator in horizontal dimension, ψ is the earth tidal potential, ρ_0 is the water density, R_s is the radiation stress gradient (calculated inside wave model), τ_w is the surface stress of wind. ρ_a is the air density, u_* is the friction velocity. $\hat{f}$ consists of all the explicit forces, and *f* is the Coriolis factor. τ_s is bottom friction.
As demonstrated in Bertin et al. (2012), the storm surge during Xynthia can only be reproduced realistically if a wave dependent surface stress is considered. Accordingly, we computed surface stress using the friction velocity u_* computed by the wave model using the approach of Bidlot et al. (2007) (calculated inside wave model)

3.2.4. Flooding Mesh and model implementation

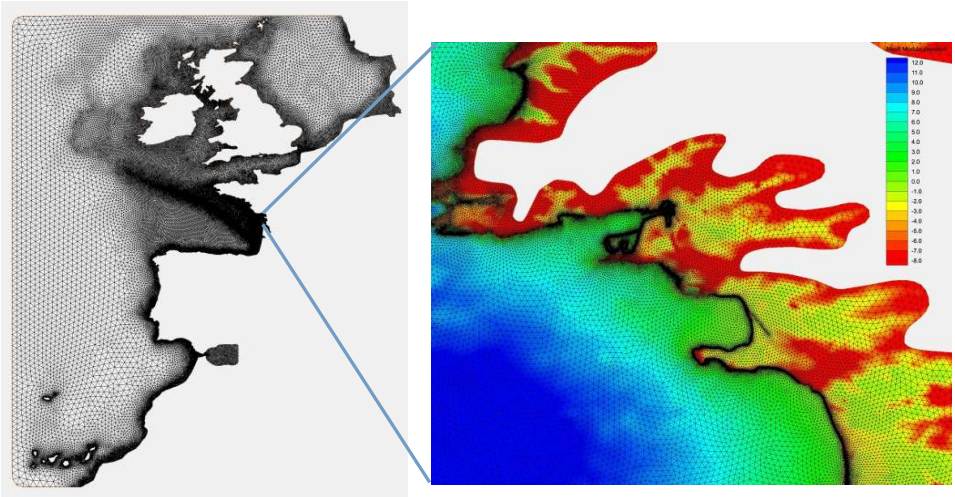

Figure2. Flooding grid of full scope (left)
Flooding grid with topography (right, with high resolution LiDAR data),

For this study, a highly refined multi-scale unstructured triangulate mesh was developed. The flooding mesh covers the whole NE Atlantic Ocean. The coarsest part of the mesh is in the west open boundary, with a resolution of 0.4 degree (up to 40 km approximately). The Bay of Biscay was refined to 0.1 degree (8 km approximately) to capture the high resolution wind data input in this area. The continental shelf break was refined to 0.03 degree (2.4 km approximately) to better represent large gradients that occur in this region. In the Pertuis Charentais, the grid was refined to 25 m along the shoreline to adequately represent breaking zones and subsequent wave setup. Finally, the grid was further locally refined along the dykes and natural barrier up to 5 m. The resulting unstructured grid has about 1,500,000 elements. High resolution topographic data were interpolated on this grid, originating from a LIDAR survey carried out a few months after Xynthia. The grid uses geographical coordinates although the equations are solved as in Cartesian coordinate using the local frame approach of Comblen et al. (2009).
SELFE is forced along its open boundary with the 17 main tidal constituents, including O1, K1, P1, Q1, M2, S2, N2, K2, 2N2, mu2, nu2, L2, M3, M4, MS4, MN4 and M6. The whole domain is forced

by 8 earth potential constituents of O1, K1, P1, Q1, M2, S2, N2 and K2. The model runs from February 22, 2010 for 7 days to get a dynamic equilibrium for water elevation. The model is then forced by atmospheric data with a resolution up to 0.25 degree and time step of 3 h derived from the model ARPEGE of Météo France. WWMII utilizes the same atmospheric forcing as SELFE and the spectral space is discretized using is 36 frequencies and 24 directions. Input and dissipation sources terms are computed using ECMWF Cycle4 parameterization. For both models, a hydrodynamic time step of 60 s was selected.

4. **Results**

4.1. Wave predictions

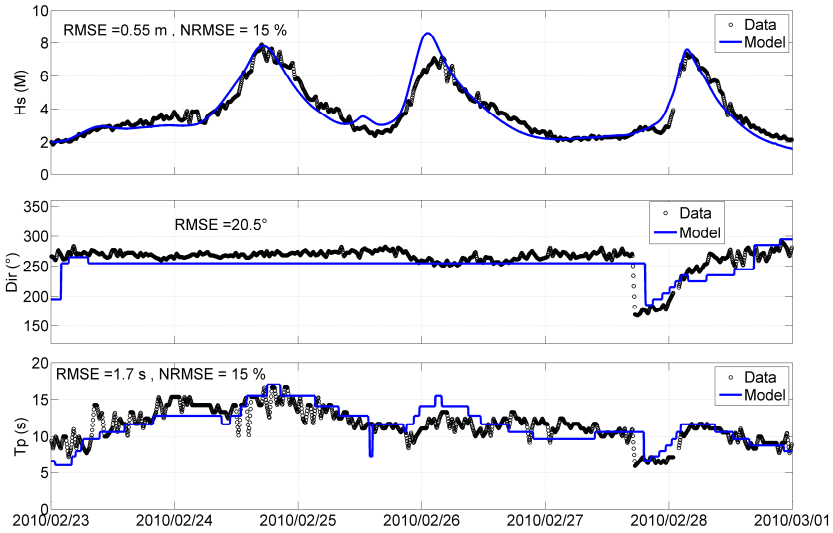

Figure 3. Validation of wave result at the Datawell Buoy offshore Oléron Island (figure 1) for Significant wave height and peak direction and period (blue dots: observed data, green line: model result).

Wave predictions were compared against data sampled offshore the Oléron Island (Figure 1). Figure 3 shows that the model is able to reproduce adequately the temporal evolution of mean wave parameters around Xynthia, with root mean square errors (hereafter RMSE) of 0.55 m, 20° and 1.7 s for significant wave height (Hs), peak direction (Pdir) and peak period (Tp), respectively. Once normalized by the data, these errors correspond to about 15 % errors for Hs and Tp. During Xynthia, the wave peak direction shifts rapidly from W (N260°) to S (N160°) while Tp drops to 6 s, but this behavior is also well captured by the model. The model globally performs very well during Xynthia, although this storm was characterized by very steep (Hs = 7 m vs Tp = 7-10s) and young waves (wave age = 9, Bertin et al., 2012).

4.2. Water levels predictions

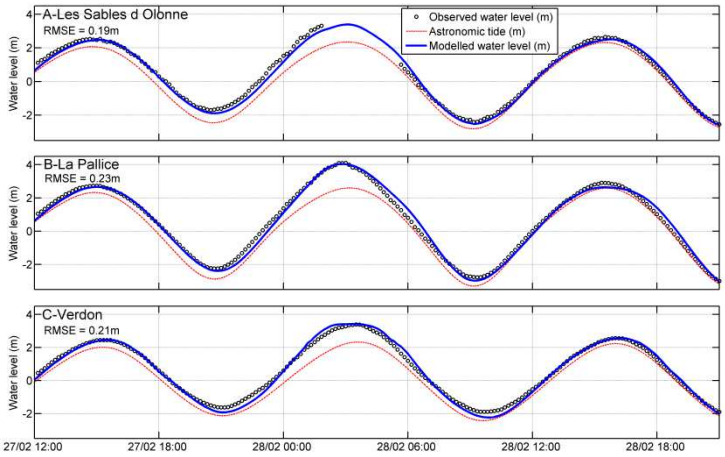

Figure 4. Validation of elevation and storm surge in La Pallice with ARPEGE wind
(black circle: observed water level, red line: astronomic tide, blue line: modelled water level,)

Model results in terms of water levels during Xynthia were compared against the available measurements at La Pallice, Pointe de Grave and Les Sables d'Olonne (Figure 1). This comparison shows that water elevations are well reproduced during Xynthia with a root mean square error of the order of 0.20 m. In more details, the maximum water levels during Xynthia are even better reproduced with RMSE below 0.1 m.

4.3. Flooding prediction

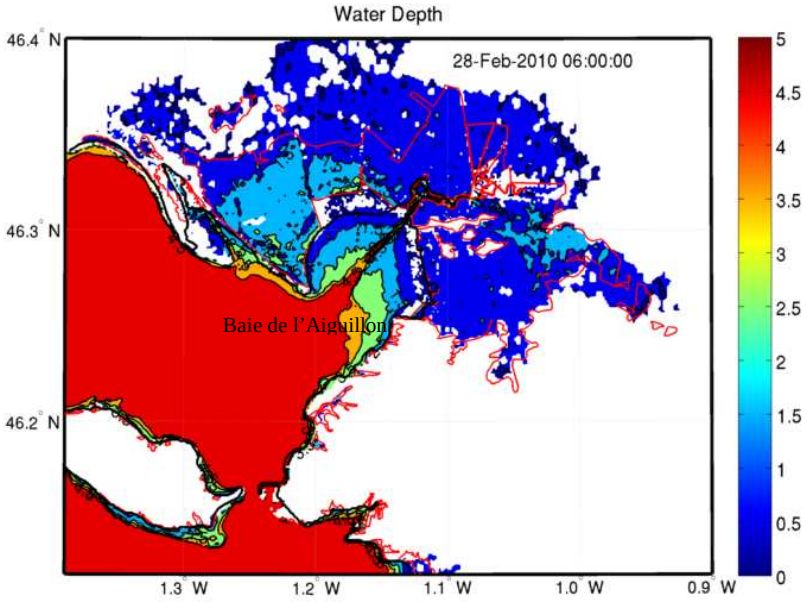

Figure 5. Maximum water depth simulated during Xynthia showing the extent of the simulated flooding compared to the observed one (red line).

Water level in La Pallice (Figure 1) hit their maximum at 3 am on the 28th February 2010 while according to our modelling results, the water started to overtop the dikes around 2am. Our preliminary results show that the extension of flooding was reasonably predicted, although the model tends to overpredict the flooding to the North of Baie de l'Aiguillon (Figure 5). Nevertheless, the extent of the flooding in the northern part of the bay was deduced from satellite images taken more than one day after Xynthia. It can thus be argued that this data underestimates the extent of the flooding in this area. Overall, the reasonable agreement between model and observation in terms of flooding extension would indicate that modeled water levels in the flooded zones are realistic. Accordingly, our modelling results suggest that low-lying wetlands protected by dykes were flooded by water depths locally reaching 3 m.

5. Discussion

5.1. Limitation of this study

This study presented preliminary results of the hindcast of the flooding associated with Xynthia. The comparison with the available water level data showed that water levels are locally well predicted, although all the considered stations are located in intermediate water depth (i.e. ~ 10m during Xynthia). Unfortunately, no water level data was available to evaluate model predictions in shallow water areas, where the storm surge is expected to grow. Alternatively, we performed a comparison between the observed and the modeled extent of the flooding during Xynthia, which revealed an overall good agreement. Maximum water levels were measured in many houses flooded during Xynthia and this data may be very useful to further validate our model predictions. Depending on these future comparisons, several improvements to the present approach could be considered, such as:

(1) As shown by Milzow and Kinzelbach (2010), flooding predictions are highly dependent on the land features (eg. roads, channels, buildings), most of which were not represented in our grid. Our grid will have to be locally refined, although there is still a threshold under which certain details cannot be represented.

(2) The representation of bottom friction presently follows a Manning friction law with values adequate for marine environments. As shown by Bunya (2010), it is expected that such values are not suitable for vegetated grounds, urbanized areas, etc. Spatially varying friction coefficients dependent on land cover will have to be considered.

(3) The topography used in our modelling study relies on a LIDAR survey carried out after the main breaches in the dykes that occurred during Xynthia were fixed. Nevertheless, our modelling results show that the extent of the flooding can be reasonably reproduced, even without breaches in the dykes. This suggests that the main part of the water flooding low lying zones overtopped the dykes rather than flew within the breaches. This hypothesis will have to be further tested, for instance through performing simulations with the breaches, most of which were well documented.

5.2. The impact of flooding in water levels

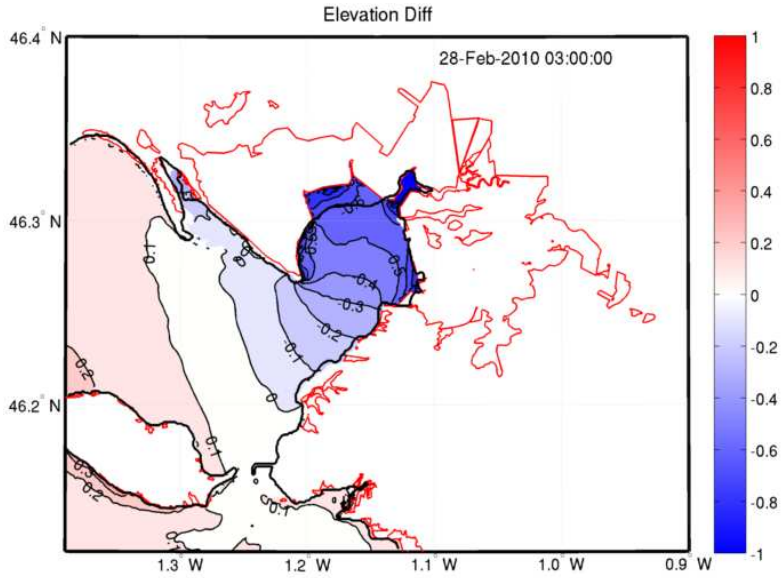

Figure 8. Difference between a simulation performed with a grid enabling flooding and a simulation without flooding, suggesting much lower water levels in the flooding case.

Although the preliminary results presented in this study suffered from some limitations listed above, the reasonable predictions of the flooding suggest that water levels are accurately predicted in our model. The comparison between water levels in a simulation enabling flooding and a simulation without flooding suggests that large differences locally appear between the two approaches. Indeed, water levels are locally 0.6 m lower when flooding is enabled. Our interpretation of this surprising phenomenon is that when flooding is not enabled, water accumulates along the dykes instead of overflowing them. These results has two main implications:

(1) Engineering approach usually employ a high resolution flooding grid forced by time series of water levels computed in a larger scale and lower resolution run. Our results suggest that this approach is only valid if a two-way nesting is employed. Otherwise the flooding in the finer grid may be strongly overestimated.
(2) After a catastrophe like Xynthia, plans for reducing flooding risks are being developed. Among the various solutions considered, raising the dyke crest would appear as an efficient solution. Nevertheless, our study suggests that this solution should be investigated with a lot of caution, as it may propagate higher water levels outside the newly protected area.

6. Conclusions

A high-resolution hindcast of the flooding associated with Xynthia was presented, relying on a fully-coupled innovative numerical modelling system. This modelling system proved to be stable and efficient, even for this challenging application. The comparison with the available data revealed that our modelling system was capable of reproducing accurately waves and water level during Xynthia in the central part of the Bay of Biscay. However, the preliminary results presented in this study have some limitations that can influent the quality of flooding predictions. Among the possible

improvements, a finer spatial resolution and the use of a more realistic bottom friction in the flooded areas will have to be tested. A comparison between a simulation with and without flooding revealed water level differences exceeding 0.6 m seaside. This result has shown to has strong implications for coastal engineering in general and management to reduce flooding risks in particular.

References

Abgrall, R. 2005. Essentially non-oscillatory Residual Distribution schemes for hyperbolic problems. Journal of Computational Physics, 214: 773-808

Bertin, X., Bruneau, N., Breilh, J., Fortunato, A. and Karpytchev, M., 2012. Importance of wave age and resonance in storm surges: The case Xynthia, Bay of Biscay. *Ocean Modelling*, 42: 16-30.

Bertin, X., Fortunato, A.B., Oliveira, A., 2008. A modeling-based analysis of processes driving wave-dominated inlets. *Continental Shelf Research*, 29: 819-834

Bidlot, J.-R., Janssen, P.A.E.M., Abdalla, S., Hersbach, H., 2007a. A revised formulation of ocean wave dissipation and its model impact. *ECMWF Technical Memorandum*, 509. ECMWF, Reading, United Kingdom.

Bilskie, M.V. and Hagen, S.C. 2012. Topographic accuracy assessment of bare earth lidar-derived unstructured meshes].[Advances in Water Resources. *Advances in Water Resources*, 52: 165-177

Brown., J. D., Spencer, T. and Moeller, I. 2007. modelling storm surge flooding of an urban area with particular reference to modelling uncertainties-- A case study of Canvey Island, United Kingdom. *Water Resources Research* 43 W06402.

Bunya, S., Dietrich, J. C., Westerink, J. J., Ebersole, B. A., Smith, J. M., Atkinson, J. H., Jesnsen, R., resio, D. T., Luettich, R. A., Dawson, C., Cardone, V. J., Cox, A. T., Powell, M. D., Westerink, H. J. and Roberts, H. J. 2010. A High-Resolution Coupled Riverine Flow, Tide, Wind, Wind Wave, and Storm Surge Model for Southern Louisiana and Mississippi. Part I: Model Development and Validation. *Monthly Weather Review* 138(2): 345-377.

Cann, B.L. 1990. Barotropic tidal dynamics of the Bay of Biscay shelf: observations, numerical modelling and physical interpretation. *Continental Shelf Research*, 10(8): 723-758.

Castaing, P., 1981. Le transfert à l'océan des suspensions estuariennes : Cas de la Gironde, thèse, université Bordeaux-1, 530.

Canizares, R., Heemink, A. W. and Vested, H. J. 1998. Application of advanced data assimilation methods for the initialisation of storm surge models Journal of Hydraulic Research 36(4): 655-674.

Chen, C., Qi, J., Li, C., Beardsley, R., Lin, H., Walker, R. and Gates, K. 2008. Complexity of the flooding, drying process in an estuarine tidal-creek salt-marsh system- An application of FVCOM, *Journal of Geophysical Research*, 113, C07052, doi:10.1029/2007JC004328.

Comblen., R., Legrand., S., Deleersnijder, E. and Legat., V. 2009. A finite element method for solving the shallow water equations on the sphere. *Ocean Modelling*, 28: 12-23

Das P. K., 1972. Prediction Model for Storm Surges in the Bay of Bengal. *Nature*, 239 : 211-213.

Dean and Dallrymple, 2001. Coastal Processes: with Engineering Applications

DDTM-17: Éléments de mémoire sur la tempête Xynthia du 27 et 28 Février 2010 en Charente-Maritime. [online] Available from: http://www.charente-maritime.equipement.gouv.fr/elements-de-memoire-xynthia-r157.html, 2011.

Dietrich, J. C., Zijlema, M., Westerink, J. J., Holthuijsen, L. H., Dawson, C., Luettich, R. A., Jensen, R. E., Smith, J. M., Stelling, G. S. and Stone, G. W. 2010. modelling hurricane waves and storm surge using integrally-coupled, scalable computations. *Coastal Engineering* 58(2011): 45-65.

Fanjul., E. Á., Gómez, B. P. and SÁNCHEZ-ARÉVALO I. R. 2001. Nivmar: a storm surge forecasting system for Spanish waters. *Scientia Marina*, 65 (1): 145-154.

Flather, R. A., 2001. Storm surges, in *Encyclopedia of Ocean Sciences*, edited by J. Steele, S. Thorpe, and K. Turekian, Academic, San Diego, California. 5: 2882– 2892

Gerritsen, H. 2005. What happened in 1953? The Big Flood in the Netherlands in retrospect. *Philosophical Transactions of the Royal Society A: Mathematical, Physical and Engineering Sciences*, 363: 1271-1291.

Geernaert, G.L., Katsaros, K.B. and Richter, K. 1986. Variation of the Drag Coefficient and Its Dependence on Sea State, *Journal of Geophysical Research*, 91(C6): 7667-7679.

Hans de Vries, Marguerite Breton, Tom de Mulder, Yannis Krestenitis, José Ozer, Roger Proctor, Kevin Ruddick, Jean Claude Salomon and Aart Voorrips 1995. A comparison of 2D storm surge models applied to three shallow European seas. *Environmental Software*, 10 (1): 23-42.

Irish., J. L., Resio, D. T. and Ratcliff, J. J. 2008. The Influence of Storm Size on Hurricane Surge. *Journal of Physical Oceanography*, 38: 2003-2013.

Jelesnianski, C. 1965. A Numberical Calculation of Storm Tides induced by a Tropical Storm Impinging on a Continental Shelf. *Monthly Weather Review* 93(6).

Jelesnianski, C. 1966. Numberical Computations of Storm Surges without Bottom Stress. *Monthly Weather Review* 94 (6): 379-394.

Johns, B., Sinha, P. C., Dube, S. K., Mohanty, U. C., Rao, A. D., 1983. Simulation of storm surges using a three dimensional numerical model: An application to the 1977 Andhra cyclone *Quart J . R. Met. SOC.* 109: 211-224.

Jones, J. E., and Davies, A. M., 1998. Storm surge computations for the Irish Sea using a three-dimensional numerical model including wave-current interaction. *Continental Shelf Research,* 18: 201-251.

Kim, S. Y., Yasuda, T. and Mase, H. 2009. Numerical analysis of effects of tidal variations on storm surges and waves. *Applied Ocean Research*. 311-322.

Mastenbroek, C., Burgers, G. and Janssen, P.A.E.M. 1992. The Dynamical Coupling of a Wave Model and a Storm Surge Model through the Atmospheric Boundary Layer, *Journal of Physical Oceanography,* 23: 1856-1866.

Milzow, C. and Kinzelbach, W., 2010. Accounting for subgrid scale topographic variations in flood propagation modelling using MODFLOW, *Water Resources Research*, 46: W10521.

Miyazaki, M., 1965. A numerical computation of the storm surge of Hurricane Carla, 1961, in the Gulf of Mexico. *Oceanography Magasine* I7 (1–2): 109–140.

Miyazaki, M. and Okada, M., 1975. Numerical simulation of storm surges in tosa bay. *Papers in Meteorology and Geophysics* 26: 55–62.

Nicolle, A., Karpytchev, M., Benoit, M., 2009. Amplification of the storm surges in shallow waters of the Pertuis Charentais (Bay of Biscay, France). *Ocean Dynamics*, 59: 921-935.

Nielsen, P., Brye, S., Callaghan, D. P., Guard, P. A., 2008. Transient dynamics of storm surges and other forced long waves *Coastal Engineering*. 499-505.

Rego., J. L. and Li, C. 2010. Nonlinear terms in storm surge predictions: Effect of tide and shelf geometry with case study from Hurricane Rita. *Journal of Geophysical Research,* 115, C06020.

Roland, A., Y. J. Zhang, H. V. Wang, Y. Meng, Y.-C. Teng, V. Maderich, I. Brovchenko, M. Dutour-Sikiric, and U. Zanke (2012), A fully coupled 3D wave-current interaction model on unstructured grids. *Journal of Geophysical Research,* 117, C00J33, doi:10.1029/2012JC007952.

Shen, J., Wang, H., Sisson, M. and Gong W. 2006. Storm tide simulation in the Chesapeake Bay using an unstructured grid model. Estuarine. *Coastal and Shelf Science*, 68: 1-16,

Shen, J., Zhang, K., Xiao, C. and Gong, W., 2006. Improved Prediction of Storm Surge Inundation with a High-Resolution Unstructured Grid Model, *Journal of Coastal Research,* 22 (6), 1309-1319.

Sheng., Y. P., Zhang, Y. and Paramygin, V. A. 2010. Simulation of storm surge, wave, and coastal inundation in the Northeastern Gulf of Mexico region during Hurricane Ivan in 2004. *Ocean Modelling* 35(2010): 314-331.

Tolman., H.L. User manual and system documentation of WAVEWATCH III version 3.14

Weisberg, R. H., and Zheng, L. 2006. A Simulation of the Hurricane Charley Storm Surge and its Breach of North Captiva Island. *Florida Scientist*, 69(00S2): 152-165,

Westerink, J.J., Luettich, R.A., Feyen, J.C., Atkinson, J.H., Dawson, C., Roberts, H.J., Powell, M.D., Dunion, J.P., Kubatko, E.J. and Pourtaheri., H. 2008. A Basin- to Channel-Scale Unstructured Grid Hurricane Storm Surge Model Applied to Southern Louisiana. *Monthly Weather Review,* 136: 833-864

Young, I., 1999. *Wind Generated Ocean Waves*, Ltd Elsevier Science Ltd.

Zhang, M. Y. and Li, Y. S. 1996. The synchronous coupling of a third-generation wave model and a two-dimentional storm surge model. *Ocean Engineering*, 23(6): 533-543.

Zanke 2012, A fully coupled 3D wave-current interaction model on unstructured grids, *Journal of Geophysical Research*, 117, C00J33, doi:10.1029/2012JC007952.

Zhang, Y.L. and Baptista, A.M., 2008. SELFE: a semi-implicit Eulerian–Lagrangian finite-element model for cross-scale ocean circulation, *Ocean Modelling*, 21 (3–4): 71–96.